Baosteel Technical Research
Volume 9, Number 3, Sept 2012, Page 18

Experimental research on hot-tearing crack sensitivity

***RUAN Xiaoming*[1], *ROBERT Pierer*[2], *SHI Chunyue*[3] *and MEI Feng*[3]**

1) Metallurgical Process Division, Research Institute, Baoshan Iron & Steel Co., Ltd., Shanghai 201900, China
2) University of Leoben, Franz-Josef-Strabe 18-A-8700 Leoben, Austria
3) Steelmaking Plant, Baoshan Iron & Steel Co., Ltd., Shanghai 201900, China

Abstract: Hot-tearing cracks usually form near the solidus temperature. It is caused by a combination of tensile stress and metallurgical embrittlement. In order to quantify embrittlement and to incorporate it in the thermal-stress analysis, many different criteria have been developed. Among them, the submerged split-chill tensile (SSCT) test is an efficient one. This paper tries to use SSCT to estimate the critical strain of hot tearing for some steels.

Key words: SSCT; hot-tearing crack; critical strain

doi: 10.3969/j.issn.1674-3458.2012.03.004

1 Introduction

In recent years, internal cracks have become the main quality problem for many domestic steelmaking plants. Such defects can cause discontinuity of mechanical properties, or even rejection of hot-rolled sheets, which greatly reduces the economic benefits. Hot-tearing crack is a typical type of internal cracks.

Crack formation is generated by a combination of tensile stress and metallurgical embrittlement. Although various mechanisms at different temperature ranges determine how solidifying metal is subject to embrittlement, hot-tearing cracks form near the solidus temperature. Embrittlement is so severe near this temperature that hot-tearing cracks form at strains on the order of only one percent, making it obvious that there exists a critical strain responsible for most of the cracks observed in cast products.

During continuous casting, the solidifying strand shell bears both mechanical and thermal loads resulting from: contraction and phase transformation; temperature gradients along the surface or across the shell; friction between strand and mold; bending and straightening; bulging; soft reduction etc. These loads act on the steel shell and generate strain. So if the total strain exceeds the critical strain value of this kind of material, cracks will occur.

In order to determine this hot-tearing critical strain, a variety of criteria and approaches, including Thermal-analysis-based Criteria, Mechanical-analysis-based Criteria and Micro-scale model-based Criteria [1], have been developed, for different approaches are required for different microstructures and metals, according to the most important phenomena which govern crack formation.

Regardless of the model formulation, developing an accurate criterion function to predict hot tears relies on measurements, such as the submerged split-chill tensile test. This experiment applies and measures a tensile load on the solidifying shell, perpendicular to the growth direction, so it matches the conditions present in hot tearing between columnar grains. The focus of this paper is to study the critical strains for different steel grades in this way.

2 Experiments

Three different kinds of steel grades were selected, including medium-carbon steel and low carbon high alloy steel. The experiment was carried out in MCC CD-Laboratory at Montan University of Leoben.

2.1 SSCT Test

Fig. 1 shows a schematic view of the SSCT test method [2-7]. A solid steel test body, split into two halves, is submerged into the liquid melt in an induction furnace. In order to control the cooling conditions and to minimize friction, the surface of the test body is coated with a thin zirconium oxide layer. A steel shell solidifies around the test body with the main crystallographic orientation perpendicular to the interface, similar to the situation in a continuous casting mould. The force between the upper and lower parts of the test sample is measured by a load cell, and the position of the lower part by an inductive position sensor. A servo-hydraulic controller controls the forces and position.

The testing parameters of the SSCT test are superheat (SH in ℃), holding time (HT in s), coating thickness (b in mm) of the test body (spray-coated with a thin zirconium oxide layer), strain rate ($\dot{\varepsilon}$ in s^{-1}) and total strain (ε_{tot} in %). The thickness of the coating influences the heat flux density (q in MW/m^2) and therefore is used to control the cooling rate, while the thickness of the shell ($s(t)$ in mm) and the temperature distribution inside the shell at the start of testing can be varied throughout the holding time. Due to the heat balance within the induction furnace, the total testing time is limited to approximately 35 s. The testing parameters used

Corresponding author: RUAN Xiaoming; **E-mail**: ruanxm@baosteel.com

in the present study are summarized in Table 1. The liquidus temperature T_L is calculated by means of JMatPro and/or IDS.

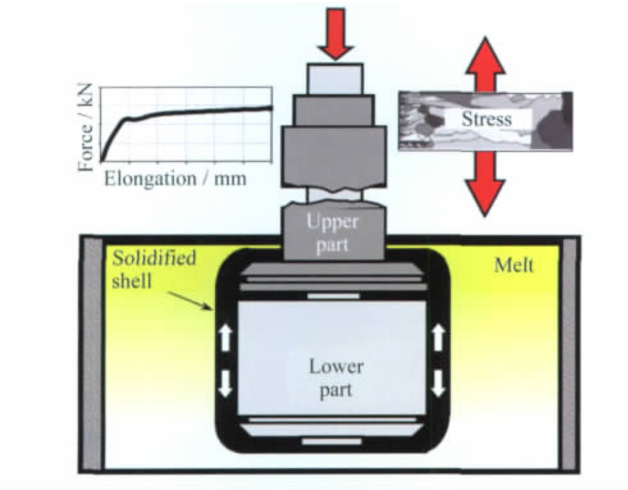

Fig. 1 Schematic diagram of SSCT test method [8]

Table 1 Requested testing parameters

Test No.	T_L /℃	SH /℃	HT/s	B/mm	$\dot{\varepsilon}$/s^{-1}	ε_{tot} /%
PL01	1 517	25	16	0.2	2×10^{-3}	0.5
PL02	1 517	25	16	0.2	2×10^{-3}	2
PL03	1 497	25	16	0.4	2×10^{-3}	0.5
PL04	1 497	25	16	0.4	2×10^{-3}	2
PL05	1 493	30	16	0.4	2×10^{-3}	0.5
PL06	1 493	30	16	0.4	2×10^{-3}	2

2.2 Steel composition

Table 2 shows the analyzed composition of the tested steel grades. A sample was taken from the melt inside an induction furnace immediately before and after testing. Remarks following the table explain and comment the results.

Table 2 Effective steel compositions of three steel grades %

Steel	Test No.	w_C	w_{Si}	w_{Mn}	w_P	w_S	w_{Al}	w_{Ni}	w_{Cr}	w_{Mo}	w_V	w_W	w_{Nb}	w_{Cequ}
Q235	P01	0.16	0.24	0.65	0.03	0.011	0.049	–	–	–	–	–	–	0.21
	P02	0.16	0.21	0.58	0.025	0.009	0.024	–	–	–	–	–	–	0.21
Ni90	P03	0.09	0.2	0.64	0.02	0.004	0.051	8.9	–	–	–	–	–	0.58
	P04	0.09	0.2	0.64	0.018	0.002	0.095	9.12	–	–	–	–	–	0.59
T92	P05	0.1	0.4	0.43	0.019	0.007	0.017	0.26	8.8	0.46	0.18	1.79	0.07	2.05
	P06	0.1	0.4	0.45	0.02	0.008	0.068	0.26	8.9	0.46	0.17	1.75	0.07	2.07

It can be seen from this table that the effective steel composition corresponds very well with the target steel composition. A mere exception is the P content out of the range in steel grade Ni90. This is led by the residual melt of Q235 within the furnace was used to build up Ni90.

2.3 Thermal analysis

The SSCT test method allows the adjustment of cooling conditions to the simulated process, by the variation of the coating thickness on the surface of the tests bodies. Within the scope of the present study, slab casting conditions with integral heat flux density of 1.25 MW/m^2 (according to a coating thickness of 0.4 mm) and bloom casting conditions with integral heat flux density of 1.45 MW/m^2 (according to a coating thickness of 0.2 mm) were simulated. The only remaining inaccuracy during testing was the superheat, because the heat balance of the small induction furnace was extremely sensitive towards temperature gradients caused by radiation of the unprotected melt surface. Before testing, the furnace was switched off and the temperature was measured by common thermocouples near the melt surface (T_{Thermo}). The superheat was adjusted to a range of 20℃ to 30℃ above liquidus. During testing, a Pt-PtRh (Type S) thermocouple measured the temperature inside the melt (T_{PtRh}) at a distance of 15 mm to 20 mm from the test body surface. This temperature was allowed to control the initial temperature. From these temperatures, $\Delta T_{SH} = SH_{PtRh} - SH_{Thermo}$ can be calculated, as is summarized in Table 3. It can be seen that ΔT_{SH} for most tests is approximately −12℃, which is within the range of that for previously conducted experiments. An exception is test PL03, in which the Pt-PtRh thermocouple measurement unfortunately broke down during submerging. In this case, T_{Thermo} is used as the initial steel bath temperature in the solidification calculation, while in all other cases, a mean value is used.

Table 3 Calculated liquidus temperature (T_L), initial temperature (T_{Thermo}), superheat, temperature during testing (T_{PtRh}) and difference between T_{PtRh} and Liquidus (SH_{PtRh}).

Test No.	T_L / ℃	T_{Thermo} / ℃	SH_{Thermo} / ℃	T_{PtRh} / ℃	SH_{PtRh} / ℃	ΔT_{SH} / ℃
PL01	1 517	1 543	26	1 531	14	−12
PL02	1 517	1 547	30	1 540	23	−13
PL03	1 497	1 548	51	–	–	–
PL04	1 497	1 543	46	1 530	33	−13
PL05	1 493	1 532	39	1 522	29	−10
PL06	1 493	1 527	34	1 516	23	−11

An important requirement to interpret the test results is detailed knowledge of the temperature distribution inside the steel shell and the shell growth during solidification. To achieve this purpose, the increase of temperature inside the test body was recorded at a defined distance from the chill-shell interface by thermocouples. As a result, the heat flux density q can be calculated at the interface between the liquid melt and the solid steel test body by means of an inverse algorithm for the solution of the heat conduction equation. Fig. 2(a) shows the plot of measured temperatures inside the test bodies for the three different steel grades.

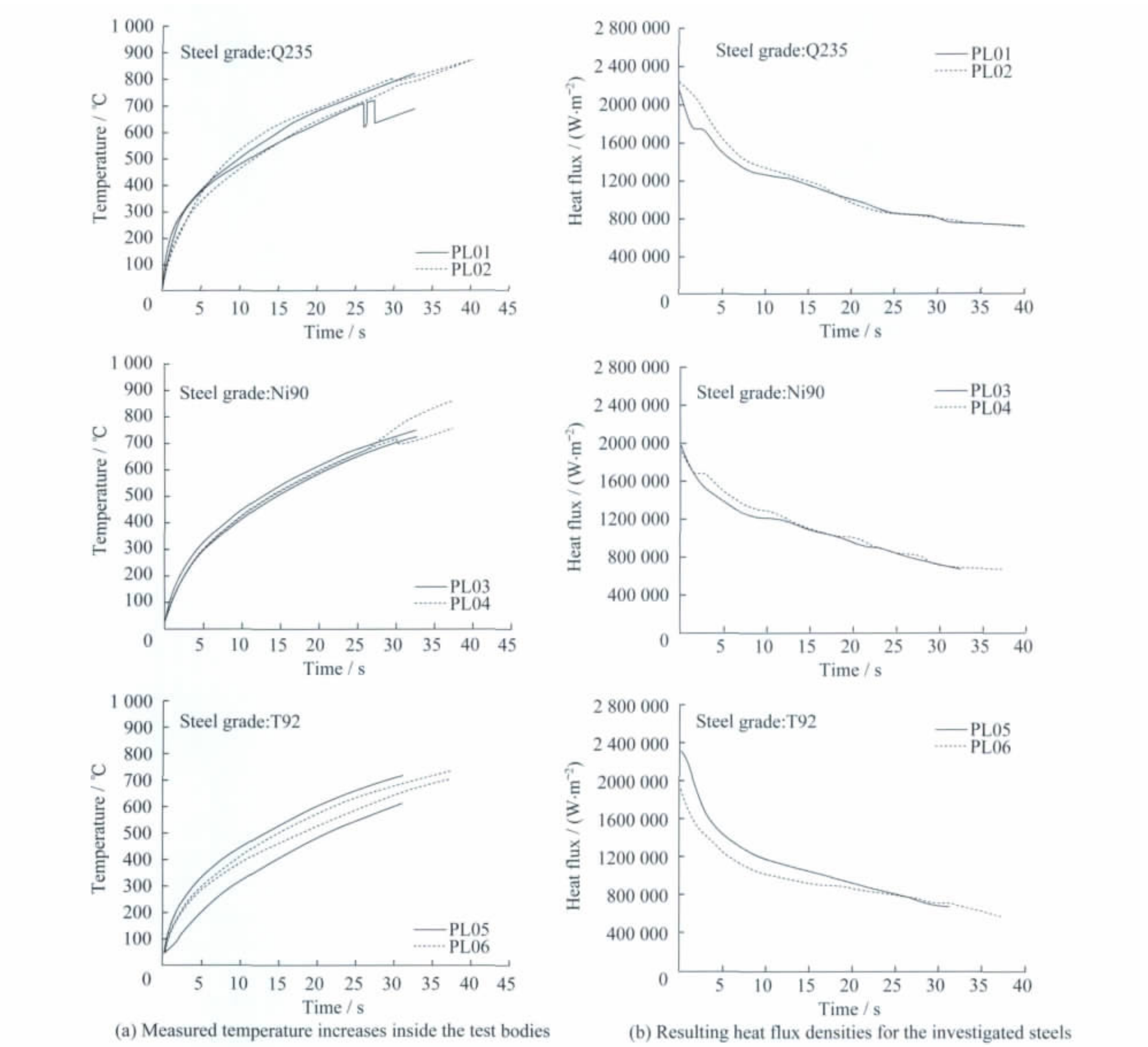

Fig. 2 Measured temperature increases inside the test bodies and resulting heat flux densities for the investigated steels

It can be seen that for Q235 and Ni90, the measured temperature increases inside the test bodies are in good accordance, while one measurement of T92 shows lower values. Among others, this behavior can be explained *e. g.* by a bad contact between the thermocouple and the test body, and will therefore not be considered in the following calculations of q. The calculated heat flux densities are illustrated in Fig. 2 (b). It shows that the maximum heat flux densities for Q235 (b = 0.20 mm) and Ni90 (b = 0.40 mm) are 2.3 and 1.8 MW/m^2, respectively. The calculated $q(t)$ of PL05 (T92) shows rather questionable high values, however it is notable that the $q(t)$ of PL06 agrees with previous results when the coating thickness is 0.40 mm. Careful thermal analysis of the experiment is carried out according to the enthalpy distribution between the chill surface and the inner side of the induction furnace determined by one-dimensional heat conduction. In the following text, the whole procedure of the thermal analysis is presented in detail for test PL02. The initial steel bath temperature (*TSB*) is 1 543℃. Fig. 2(a) shows the measured temperatures during the SSCT test. The temperature, recorded by two thermocouples (THC01 and THC02), increases inside the test body and serves as the input data for the calculation of the heat flux density (illustrated in Fig. 2(b)). The result of the solidification calculation is the temperature distribution in the melt during the SSCT test. This distribution as a function of time and in conjunction with the results from a microsegregation model (fraction of solid vs. temperature) allows the calculation of shell growth during the experiment.

Finally, this calculation procedure enables the determination of the shell growth during the SSCT test. Fig. 3 illustrates the calculated shell growth as a function of solidification time for the isotherms corresponding to solid fractions of 0 and 1. In addition, the measured shell thickness together with the scatter band of the measurement is illustrated. In previous studies it was shown that the measured shell thickness was in good agreement with a solid fraction of approximately 0.2. Apart from the comparison of the measured (T_{PtRh}) and calculated temperature of the melt, the comparison of measured and calculated (f_S = 0.2) shell thickness is an important basis for the reliability of the thermal analysis. The duration of submerging and the duration of emerging are both approximately 2 s. The holding time for the present study is 16 s and the total strain for PL02 is 2.0%. Thus, with a strain rate of 2×10^{-3}/s, the testing time results in 10 s, leading to a total solidification time of 30 s.

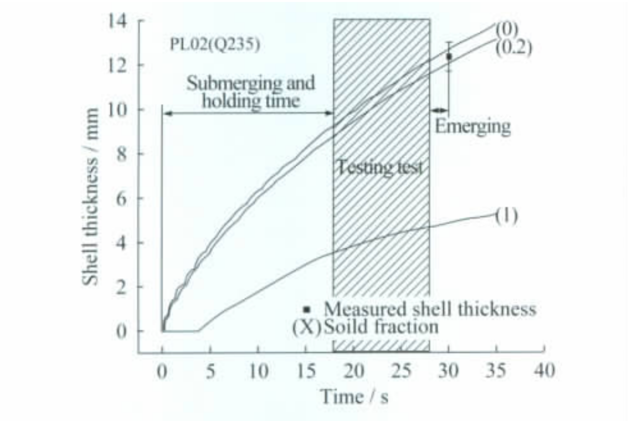

Fig. 3 Calculated and measured shell thickness as a function of solidification time together with the different stages during the SSCT test PL02

2.4 Metallographic analysis

The evaluation of hot tears is done by separation of the solidified shell from the test body. In doing so, 16 samples are cut from the circumference of the shell and are finally polished and etched. This procedure is schematically shown in Fig. 4 (left-hand side). The solidified steel shell around the test body is illustrated together with the samples and the polished and etched metallographic specimen. 8 out of these 16 specimens are finally investigated in a metallographic examination in which the hot tears are counted (Number of Hot Tears, *NHT*) and their lengths (Length of Hot Tears, *LHT*) are measured. In addition, the distance from the chill-shell interface (Distance from Interface, *DfI*) is determined.

The evaluation procedure of these parameters is illustrated in Fig. 4 (right-hand side). The determination of *NHT* and *LHT* is performed according to the following equations:

$$NHT = \frac{1}{N_{\text{Micrograph}}} \cdot \sum_{i}^{k} N_i$$

$$LHT = \frac{1}{N_{\text{Micrograph}}} \cdot \sum_{i}^{k} L_i$$

In these two equations, $N_{\text{Micrograph}}$ is the number of analyzed micrographs (mainly eight micrographs) and k denotes the individual hot tear. In addition, the ratio of LHT/NHT can be determined, which represents the average tear length *ATL*.

3 Results and discussion

Fig. 5 summarizes the results for steel grade Q235. The left diagrams show the shell growth as a function of solidification time. Additionally, the time range (testing period) of the tensile test is highlighted to stress the shell growth during the experiments and therefore the non-isothermal conditions are similar to those in the continuous casting process. It can be seen from these diagrams that the measured shell thickness at the end of the experiments tends to conform to a solid fraction of 0.2. The right-hand diagrams show the distribution of *NHT* (please note that this distribution only refers to the starting point-by means of *DfI*-of the detected hot tears, see Fig. 4) for tests PL01 and PL02 with total strains of 0.5% and 2.0% respectively. From these two diagrams, it can be concluded that a higher total strain results in more hot tears.

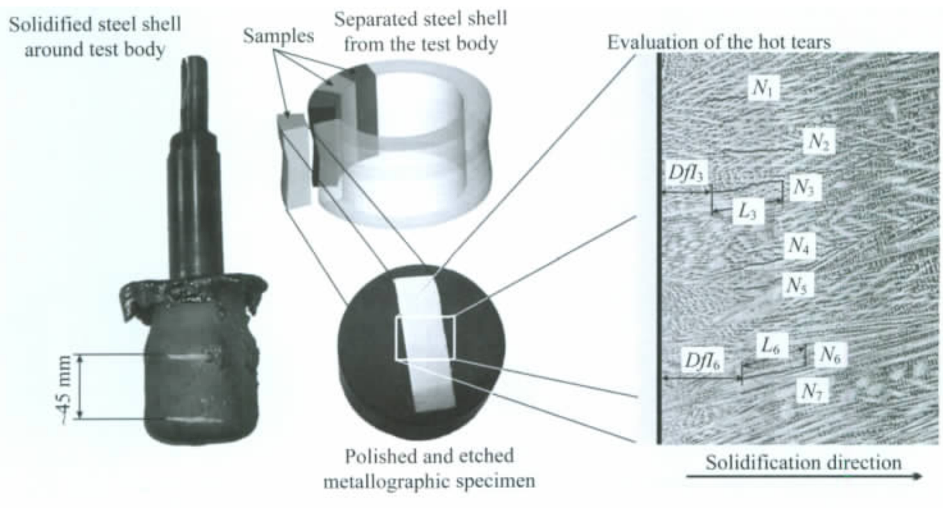

Fig. 4 Schematic illustration of metallographic specimen preparation and detailed view of a micrograph including hot tears

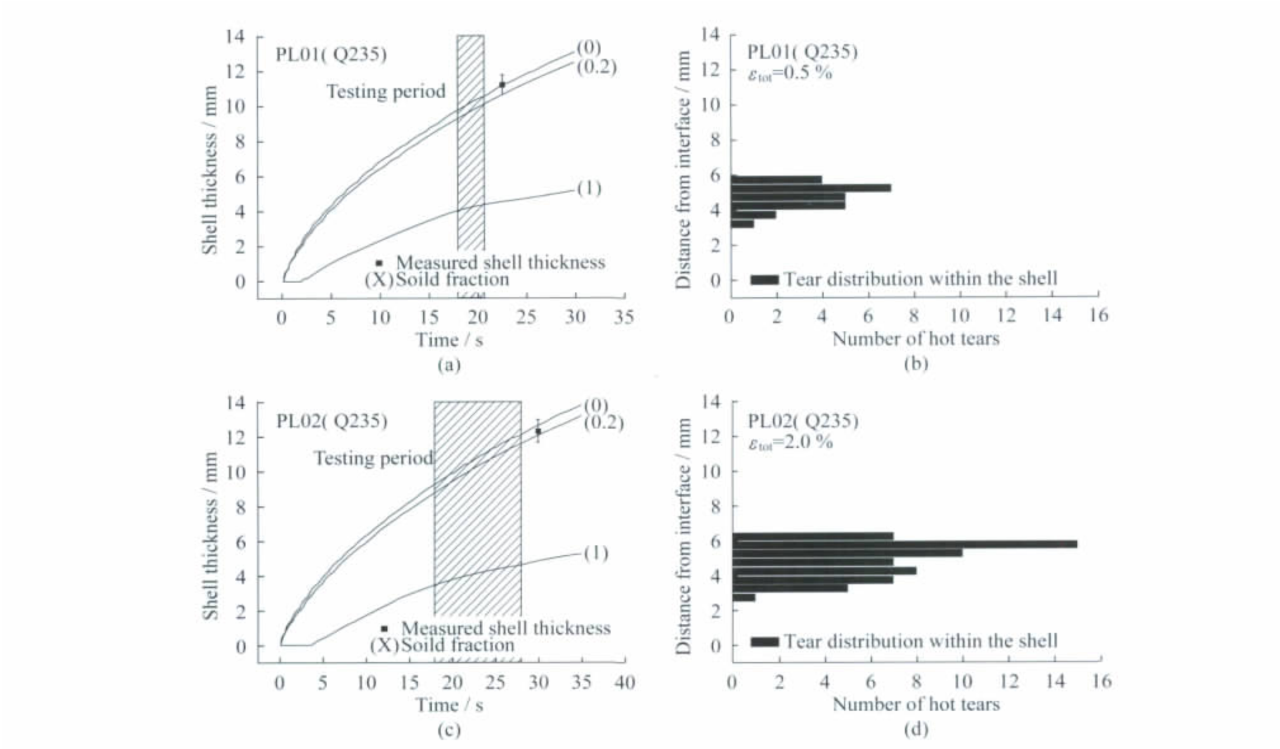

Fig. 5 Calculated shell growth and distribution of hot tears for tests PL01 and PL02 (Q235)

The same situation as described above is illustrated for Ni90 and T92. Similar to the above presented results of Q235, the shell growth and the distribution of *NHT* are illustrated in these diagrams. From the solidification calculations, it can be concluded that the measured and calculated ($f_S = 0.2$) shell thicknesses tend to agree with each other. Likewise, the distribution of *NHT* within the shell shows a similar trend in all cases with a maximum of detected hot tears at a certain position from the interface. Both steel grades show an increasing hot tearing tendency with the increase of the total strain.

Fig. 6 shows typical hot tears (white arrows) generated when a total strain of 2.0% is applied (PL02, Q235). Generally, these hot tears are segregated hot tears. In the present study it was not possible to initiate open hot tears within the mushy zone. Additionally, the position of T_S and T_L at the begin $T(1)$ and end $T(2)$ of the tensile test is illustrated in Fig. 6. It can clearly be seen that the detected cracks (hot tears) are generated within the mushy zone.

Besides *NHT* and *DfI*, the length of hot tears (*LHT*) was measured. This parameter means a total crack length per micrograph. Hence, the ratio of *LHT/NHT* results in an average tear length (*ATL*) of the investigated tests. Fig. 7 summarizes the results of these three parameters for all six experiments. Additionally, an error bar is included in the diagrams, which is the standard deviation from the eight measurements (micrographs) per test in the case of *NHT* and *NHT*. The scatter band at *ATL* is the result of the standard deviation of all measured hot tears (length *L*) per test.

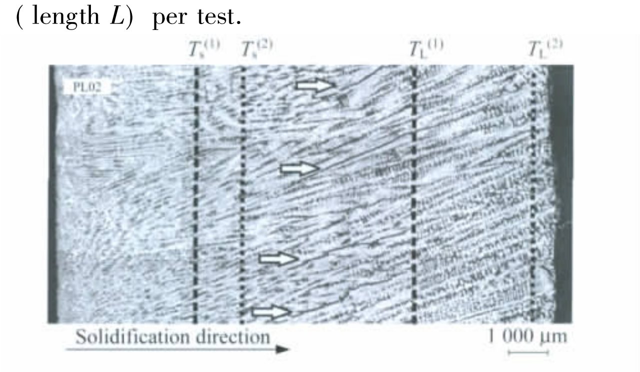

Fig. 6 Micrograph of test PL02 (Q235) including segregated hot tears

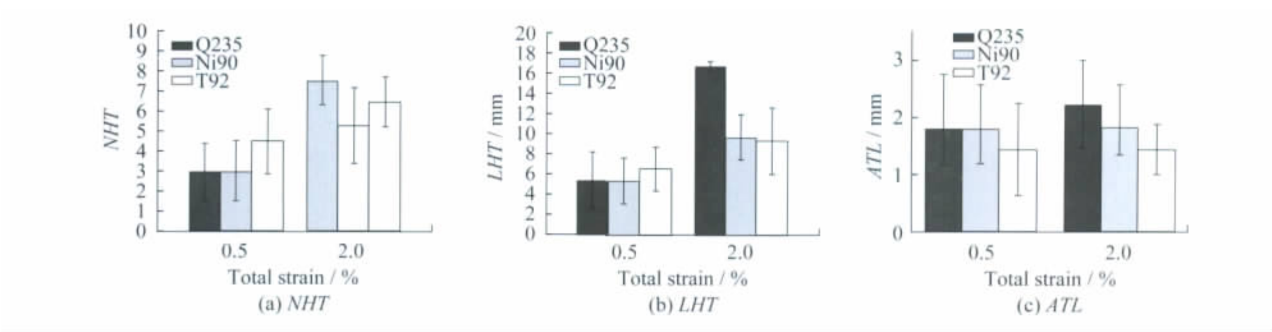

Fig. 7 *NHT*, *LHT* and *ATL* for the three different steel grades and for total strains of 0.5% and 2.0%

Fig. 7(a) shows *NHT* for all steel grades and for total applied strains of 0.5% and 2%. It can be seen that a total applied strain of 0.5% results in hot tearing in all cases. Q235 and Ni90 show the same numbers of hot tears, whereas T92 seems to be more prone to hot tearing in terms of *NHT*. When the equivalent carbon content (C_{equ}) of these three steel grades is taken into consideration, crack susceptibility increases with the increase of C_{equ} in steel.

As is expected, increasing the strain to 2% results in an increase of *NHT* for all steel grades. However, the greatest increase is obtained for Q235 and the smallest increase is found for Ni90. Although T92 shows the biggest number of hot tears at $\varepsilon_{tot} = 0.5\%$, an increase of the strain up to 2% results in *NHT* between Q235 and Ni90. Similar behavior can be found in terms of *LHT* (see Fig. 7(b)). Q235 and Ni90 show lower values of *LHT* than T92 when $\varepsilon_{tot} = 0.5\%$. Increasing the strain (ε_{tot}) to 2.0% raises *LHT* in all cases, and Q235 shows the highest value. However, the other two steel grades show a rather moderate increase of *LHT* with the increase of strain. Thus, crack sensibility seems more related to the carbon content. As for the average tear length *ATL* (see Fig. 7 (c)), it appears that increasing the strain from 0.5% to 2.0% generally results in minor tear growth.

In order to determine the critical strain of hot tearing, an assumption with respect to the extent of hot tearing in terms of *NHT* must be made, i. e. the tolerable *NHTtol* must be defined. When *NHTtol* is assumed to be 1, the critical strains of hot tearing are lower than 0.5% for all the three steel grades. However, an exact value cannot be determined with the two determined values (0.5% and 2.0%) per test. Fig. 8 shows the predicted situation for Q235 with a tolerable *NHT* of 1, a scatter band of +/−1 and total strains of 0.25% and 0.75%.

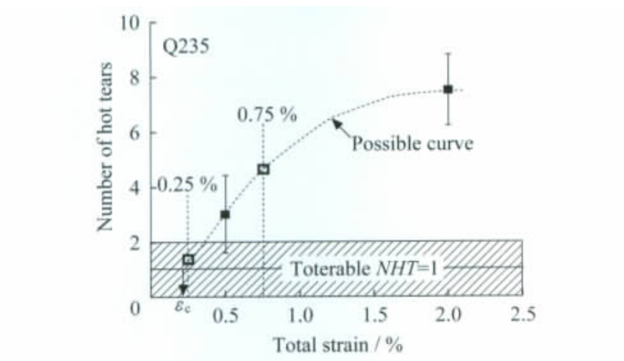

Fig. 8 Procedure to determine the critical strain of hot tearing with *NHTtol* = 1

4 Conclusions

(1) SSCT test is an effective method to study the crack sensitivity of steel under the conditions of continuous casting at laboratory.

(2) With a total strain of 0.5%, crack susceptibility is related to the C_{equ} in steel, but as the strain increases up to 2%, crack sensibility is more relative with the carbon content in steel.

(3) In order to determine the critical strain of hot tearing, it is necessary to conduct further experiments to study the situations with total strains of 0.25% and 0.75%.

(4) As for the SSCT test, it is necessary to make more efforts to get an accurate total strain, such as 0.1% or less.

References

[1] Thomas B G. Modeling of hot tearing and other defects in casting processes [J]. ASM Handbook, 2009, 22: 362 – 374.

[2] Xia G, Zirngast J, Hiebler H, *et al*. High temperature mechanical properties of in situ solidified steel measured by the new SSCT test [C]//Proc. 1st Conference on Continuous Casting of Steel in Developing Countries. Beijing: The Chinese Society for Metals, 1993: 200 – 210.

[3] Bernhard C, Hiebler H and Wolf M. Experimental simulation of subsurface crack formation in continuous casting [J]. Revue de Metallurgie, Cahiers d'Informations Techniques (France). 2000, 97(3): 333 – 344.

[4] Hiebler H, Zirngast J, Bernhard C, *et al*. Inner crack formation in continuous casting: stress or strain criterion [C]//Proc. Steelmaking Conference. Chicago: Iron and Steel Society/AIME, 1994, 77: 405 – 416.

[5] Bernhard C, Hiebler H and Wolf M. Simulation of shell strength properties by the SSCT test [C]//Proc. Conference on Continuous Casting of Steel in Developing Countries. Wuhan: The Chinese Society for Metals, 1997: 224 – 229.

[6] Hiebler H and Bernhard C. Mechanical properties and crack susceptibility of steel during solidification [J]. Steel research, 1999, 69(8+9): 349 – 355.

[7] Bernhard C, Hiebler H and Wolf M. Simulation of shell strength properties by the SSCT test [J]. ISIJ, 1996, 36 (Supplement): 163 – 166.

[8] Bernhard C, Pierer R, Tubikanec A, *et al*. Experimental characterization of crack sensitivity under continuous casting conditions [C]//Continuous-casting Innovation Session. Linz: Voest-Alpine Industrieanlagebau, 2004: 2 – 9.


RUAN Xiaoming


ROBERT Pierer


SHI Chunyue


MEI Feng